Organic & Biomolecular Chemistry

Accepted Manuscript

ROYAL SOCIETY OF CHEMISTRY

www.rsc.org/obc

Theoretical investigations toward the reaction between 1,4-dithiane-2,5-diol and azomethine imines: mechanisms and diastereoselectivity

Linjie Zheng,[‡] Yan Qiao,[*,†] Mengxue Lu,[‡] and Junbiao Chang[*,†]

[†]Department of Pathophysiology, School of Basic Medical Sciences, and [‡]The College of Chemistry and Molecular Engineering, Zhengzhou University, Zhengzhou, Henan 450001, China.

E-mail: yanqiao@zzu.edu.cn, changjunbiao@zzu.edu.cn

Abstract

In the present study, mechanistic insights into the domino reaction between 1,4-dithiane-2,5-diol and azomethine imines was derived from the computational study with B3LYP and M06-2X functionals. On the whole, the domino process comprises two consecutive reactions: cleavage of 1,4-dithiane-2,5-diol leading to mercaptoacetaldehyde and [3 + 3] cycloaddition of mercaptoacetaldehyde with azomethine imines. The cleavage of 1,4-dithiane-2,5-diol can take place via multiple possible pathways (1A-1E), and pathway 1E in which double-methanol molecules mediate the proton transfer process is most energetically favorable with an energy barrier of 19.9 kcal/mol. For the [3 + 3] cycloaddition, three possible pathways (2F-2H) were explored. The calculated energy profiles reveal that pathway 2H with activation energies ranging from 6.9 to 10.2 kcal/mol are more energetically favorable than pathway 2F and 2G. Specifically, pathway 2H comprises three reaction steps: deprotonation of mercaptoacetaldehyde by DABCO allows for the formation of thiol anion, which subsequently nucleophilic attack on azomethine imines followed by intramolecular cyclization resulting into the final products. The calculated results are in agreement with the experimental observations that the reaction can proceed most efficiently in the presence of both DABCO and methanol. Furthermore, hydrogen bonding interaction is identified to be the main factor determining the observed diastereoselectivity The current systematic theoretical study gives a full scenario on the reaction between 1,4-dithiane-2,5-diol and azomethine imines catalyzed by

DABCO, and thus provide some valuable clues for further investigation and development of this important kind of reaction.

Introduction

Organosulfur compounds play important roles in the biochemistry of almost all living organisms and inevitably present in many synthetic drugs as well as bioactive natural products.[1-3] Due to the important pharmaceutical applications, the synthetic methodologies for them have attracted more and more attention. In particular, the catalytic C–S bond formations have been researched by many chemists in modern synthetic organic chemistry, and significant progress has been achieved in the past decades.[4] Numerous metal-catalyzed and organocatalytic C–S bond formations, e g. sulfa-Michael reactions[5-12], 1,2-[13,14], 1,6-[15,16], and γ-additions[17,18] of sulfur nucleophiles, desymmetrization of anhydrides[19-21], aziridines[22-24], oxetanes[25], and azlactones[26,27] as well as sulfenylation[28-30] and thioesterification reactions[31-33] have been explored extensively.

It is worth mentioning that Wang et al. recently reported an unprecedented [3 + 3] cycloaddition of 1,4-dithiane-2,5-diol **1** with azomethine imines **2** catalyzed by DABCO **3** to construct the dinitrogen-fused sulfur-containing heterocycles **4** (shown in Scheme 1a).[34] This stepwise [3 + 3] cycloaddition methodology is a complementary strategy to [4 + 2] cycloaddition for the synthesis of six-membered heterocyclic compounds.[35] More importantly, the dinitrogen-fused and sulfur-containing products **4** obtained from this reaction is very interesting and

valuable, since the dinitrogen-fused heterocycles are inherently typical motifs present in many pharmaceuticals, agrochemicals, bioactive compounds as well as in other useful chemicals.[36,37] The current reactions give access to novel structures combining two important functional groups, so it can be viewed as a combinatorial chemistry method, an important strategy used in medicinal chemistry. Besides, the cycloaddition reactions based on azomethine imines and 1,4-dithiane-2,5-diol are practical and can proceed efficiently under mild conditions in good yields with excellent diastereoselectivities. So no matter for the methodology for construction of heterocycles, or for the new structural folds being formed, the cycloaddition reactions shown in Scheme 1a is very important and merits attention. However, some curious phenomena observed in the experiments remain to be explored. For example, (1) 1,4-dithiane-2,5-diol **1** is widely used in organic synthesis and it is generally believed to initially cleave to form mercaptoacetaldehyde **5** (Scheme 1b), which could then react with other reactant substrates.[34,38-40] However, how is mercaptoacetaldehyde being formed has never been investigated and the detailed reaction process remains elusive. (2) The reaction rate is highly dependent on the base and solvent used. Without base and protic solvent, the reaction can only proceed very slowly in two days with low yields. In the presence of base and absence of protic solvent, the reaction can proceed more smoothly within an hour in good yield with high diastereoselectivities. Finally, when both base and protic solvent are present, the reaction can proceed very efficiently within fifteen minutes in excellent yield with admirable diastereoselectivities.[34] Based on these experimental observations, we may

ask why the reaction proceeds more efficiently in the presence of base (e.g., DABCO) and protic solvent (e.g., MeOH). What are the exact roles of base and protic solvent in the reactions?

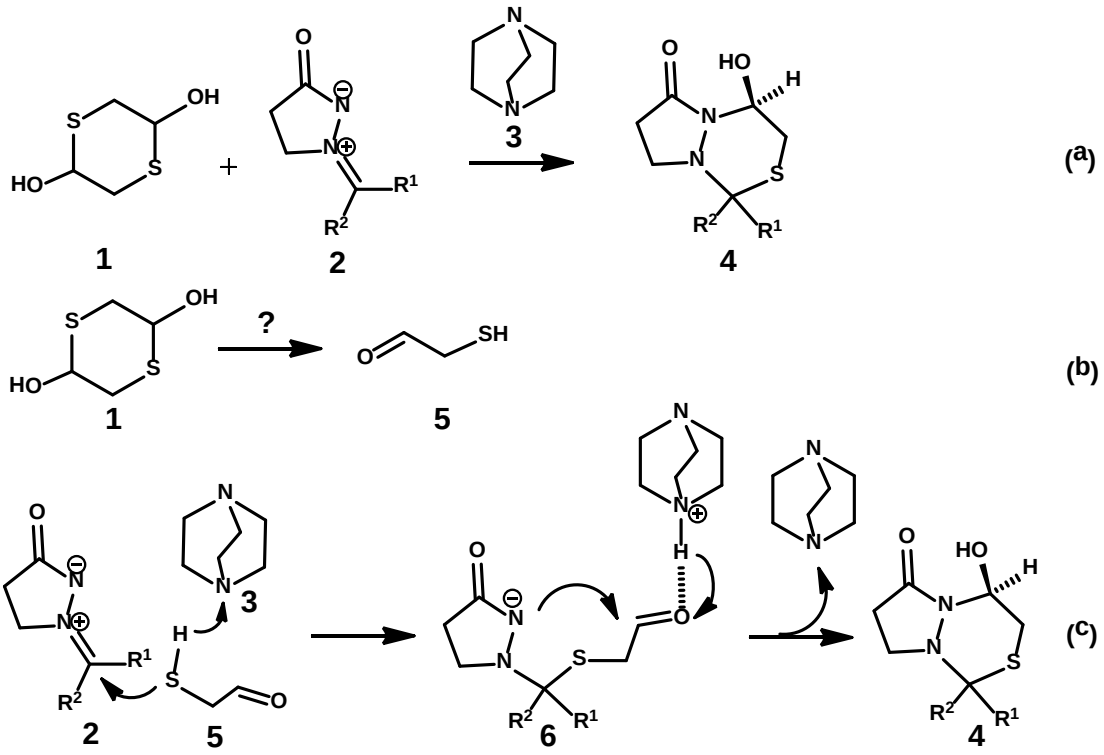

Scheme 1. DABCO-catalyzed [3 + 3] cycloaddition between 1,4-dithiane-2,5-diol and azomethine imines.

In the original experimental report, Wang et al. proposed that DABCO is a catalyst, and its tertiary amine could enhance the nucleophilicity of mercaptoacetaldehyde, which could then react with azomethine imine.[34] So DABCO is supposed to function as a general base to abstract the hydrogen from the mercapto group of mercaptoacetaldehyde (Scheme 1c), but if DABCO has some other functions except for the role of a base is unclear. In addition, the detailed reaction mechanisms and the corresponding structures of transition states and intermediates are unclear. Prompted by all of these questions and pushing for a deeper understanding of the

reaction mechanism for this kind of reaction, herein we performed DFT calculations, a method of choice for the cost-effective treatment of various chemical systems with high accuracy,[41-53] to provide mechanistic insights into this important [3 + 3] cycloaddition reaction.

In the present study, a representative reaction in which R^1=Ph and R^2=H (shown in Scheme 1) were selected as our model reaction. The detailed reaction mechanism as well as the diastereoselectivity will be discussed in the following.

Computational details

All theoretical calculations were performed using the Gaussian 09[54] suite of programs. The geometrical structures of all the stationary points in the energy profiles were optimized at the B3LYP/6-31G(d, p) level[55,56] in the methanol solvent using IEFPCM solvent model.[57,58] The Berny algorithm was employed for both minimizations and optimizations to transition states.[59] The corresponding vibrational frequencies were calculated at the same level to take into account the zero-point vibrational energy (ZPE) and to identify whether the structure is a transition state or a minimum. We confirmed that all reactants and intermediates had no imaginary frequencies, and each transition state had only one imaginary frequency. Intrinsic reaction coordinate (IRC) calculations,[60,61]at the same level of theory, were performed to ensure that the transition states led to the expected reactants and products. We then refined the energy by performing single-point energy calculations at the M06-2X/6-311+G(d, p) level[62-64] based on the B3LYP/6-31G(d, p) optimized

structures and ZPE corrections. In the following discussion, the energies obtained by addition of ZPE correction at B3LYP/6-31G(d,p) level to the corresponding single-energy at the M06-2X/6-311+G(d, p) level in the solvent are used.

Results and Discussion

According to the calculated results, the domino process comprise two consecutive reactions and can take place via multiple competing reaction pathways (see Schemes 2–8). The following discussion on the reaction mechanisms has been divided into two separate sections: 1) Generation of the mercaptoacetaldehyde; 2) [3 + 3] cycloaddition between mercaptoacetaldehyde and azomethine imines. In the following, we will discuss the two sections in detail.

1. Generation of mercaptoacetaldehyde. 1,4-dithiane-2,5-diol should first cleave to form mercaptoacetaldehyde, which is then able to react with azomethine imines. In the present study, we characterized several reaction pathways (1A, 1B, 1C, 1D, and 1E) for the cleavage of 1,4-dithiane-2,5-diol.

1. 1. Direct cleavage of 1,4-dithiane-2,5-diol. As shown in Scheme 2, in the absence of catalyst, the cleavage of 1,4-dithiane-2,5-diol (**R1**) can take place via one stepwise (pathway 1A) or one one-step (pathway 1B) mechanism. For pathway 1A, reactant **R1** is initially opening *via* a four-membered ring transition state **TS1A** leading to intermediate **M1A** (as shown in Scheme 2). In **TS1A**, the C1–S1 bond is breaking, and simultaneously the proton H1 attached with oxygen O1 is being transferred to the

sulfur S1 atom. The energy analysis reveals that this step is endothermic and requires a significant activation energy of 46.6 kcal/mol. Followed by the generation of intermediate **M1A** is the breaking of the second C–S bond via transition state **TS2A**. Likewise, accompanied by the C2–S2 bond breaking in **TS2A**, the proton H2 attached with O2 is also transferred to S2 atom and thus generate two molecules of mercaptoacetaldehyde. **TS2A** is also a four-membered transition state with an extremely high energy barrier of 52.3 kcal/mol. The high energy barriers of **TS1A** and **TS2A** indicate that pathway 1A is not energy favorable.

In addition to pathway 1A, an alternative one-step pathway for cleavage of **R1** can also be envisaged (shown as pathway 1B in Scheme 2), whereby the two C–S bonds are simultaneously breaking via transition state **TS1B**. Noteworthy, the proton transfer process in pathway 1B is very different from that in pathway 1A. In pathway 1A, the sulfur atom abstracts the hydrogen atom from its neighboring oxygen atom, while in pathway 1B the sulfur atom abstracts the hydrogen from the other oxygen atom. As was shown in Scheme 2, the activation energy barrier for this process was calculated to be 38.6 kcal/mol, which is lower than that of pathway 1A (52.3 kcal/mol). The lower activation energy for pathway 1B relative to pathway 1A is attributed to the reduced ring strain in transition state **TS1B**.

As described above, it is difficult for the reaction to occur via pathway A and B due to the significant energy barriers, which is contradictory with the fact that the reaction can go through easily at room temperature. Therefore, we need to identify other possible reaction pathways.

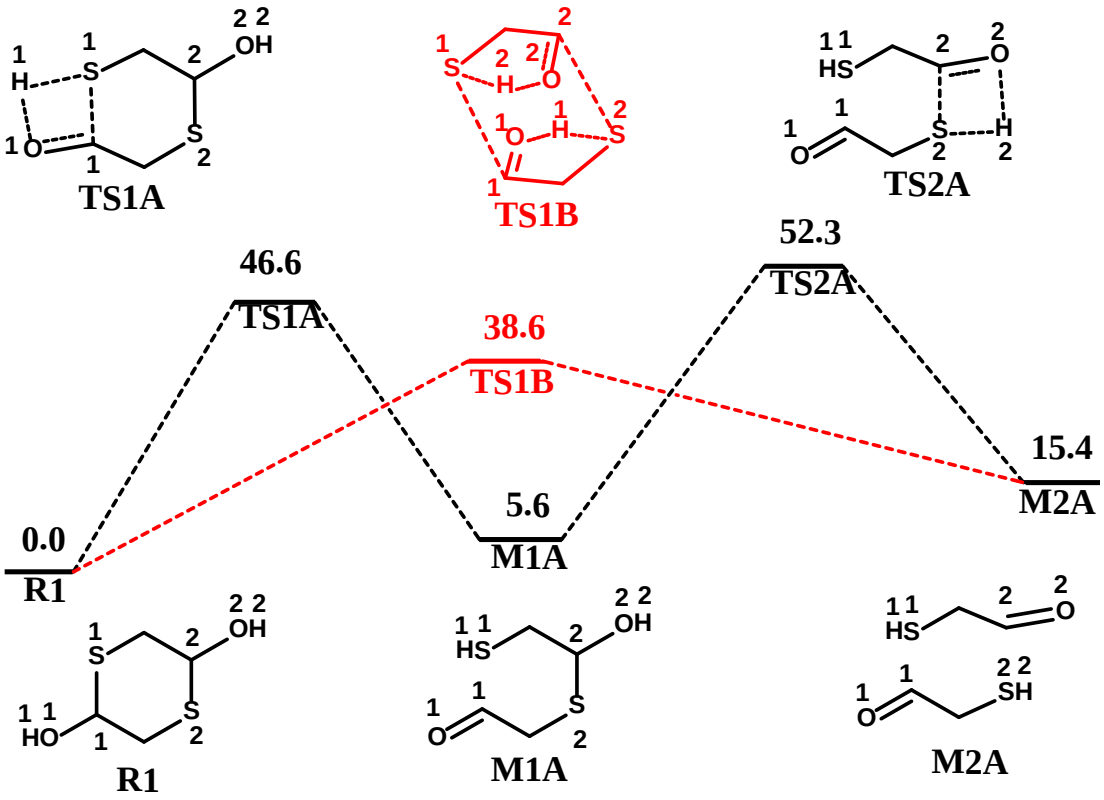

Scheme 2. The energy profile for cleavage of 1,4-dithiane-2,5-diol (pathways 1A and 1B with black and red color respectively).

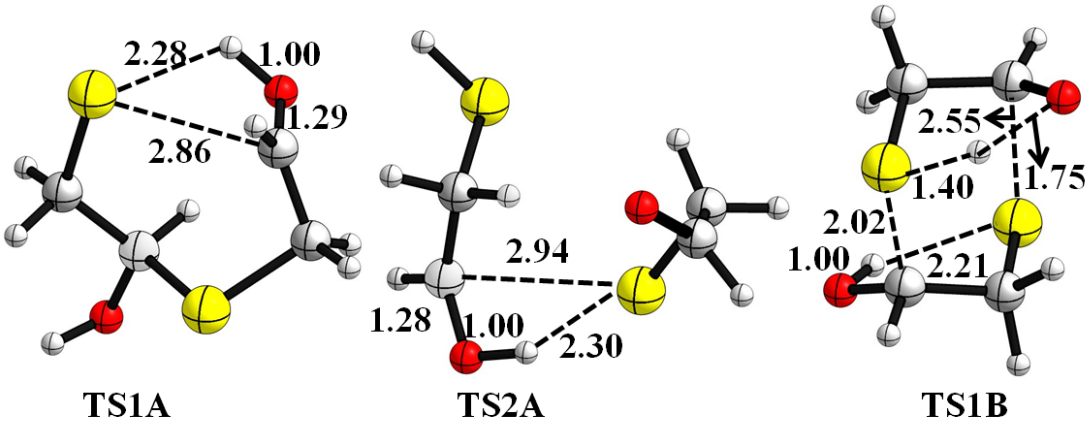

Figure 1. The optimized transition state structures for pathways 1A and 1B, selected distances are shown in Å.

1.2. **DABCO-catalyzed cleavage of 1,4-dithiane-2,5-diol.** It was reported that in the presence of DABCO, the reaction can proceed smoothly within an hour.[34] So we speculate that DABCO is likely to have the ability to catalyze the cleavage of

1,4-dithiane-2,5-diol. The mechanistic proposal for DABCO-catalyzed cleavage of 1,4-dithiane-2,5-diol is shown in Scheme 3 (pathway 1C) and it has been confirmed through the calculation. As can be seen, DABCO-catalyzed cleavage of 1,4-dithiane-2,5-diol consists of four steps. In the first step, DABCO acts as a nucleophile to attack on C1 of **R1** via transition state **TS1C**, in which the C1–S1 bond is breaking (C1–S1 bond distance: 2.84 Å) and the C1–N bond is forming (C1–N bond distance: 2.28 Å). Obviously, the first step is a S_N2 type reaction, and the activation energy for this step is calculated to be 23.2 kcal/mol. In the generated intermediate **M1C**, the C1–N bond is formed and C1–S1 bond is completely broken. Followed by the formation of intermediate **M1C** is the elimination of DABCO and proton H1 transfer from oxygen O1 to sulfur S1. This reaction process go through transition state **TS2C** and requires an activation energy of 4.4 kcal/mol. In the formed intermediate **M2C**, the C1–N bond is broken and DABCO is released.

Subsequently, in order to initiate the next nucleophilic attack to break the C2–S2 bond, DABCO should be repositioned to fit the new reaction coordinate. Herein, intermediate **M2C′** was identified, in which DABCO is at an appropriate position to attack on the carbon C2 atom. Notably, the nucleophilic attack of DABCO on the carbon C2 atom occurs concertedly with the C2–S2 bond breaking event. Apparently, the third step also follows the S_N2 type reaction mechanism. The transition state involved in this step is **TS3C**, in which the C2–S2 bond is 2.88 Å and the C2–N bond is 2.55 Å. The energy of transition state **TS3C** is 24.7 kcal/mol relative to the reactant **R1+R3**. In the formed intermediate **M3C**, the C2–S2 bond is totally broken and the

C2–N bond is formed. Then, the elimination of DABCO via transition state **TS4C** give rise to two molecules of mercaptoacetaldehyde. Similar with **TS2C**, the elimination of DABCO in **TS4C** is also coincident with the proton H2 transfer from O2 to S2. The activation energy for **TS4C** is calculated to be 11.6 kcal/mol, indicating that it is easy to occur.

In conclusion, the DABCO-catalyzed cleavage of 1,4-dithiane-2,5-diol comprise four steps and the third step associated with **TS3C** is rate-limiting. Therefore, the highest energy barrier in pathway C amounts to 25.1 kcal/mol (from the lowest-energy stationary point **M1C** to the highest-energy transition state **TS3C**), which is not a high barrier at room temperature. The optimized transition state structures of **TS1C**, **TS2C**, **TS3C** and **TS4C** are shown in Figure 2.

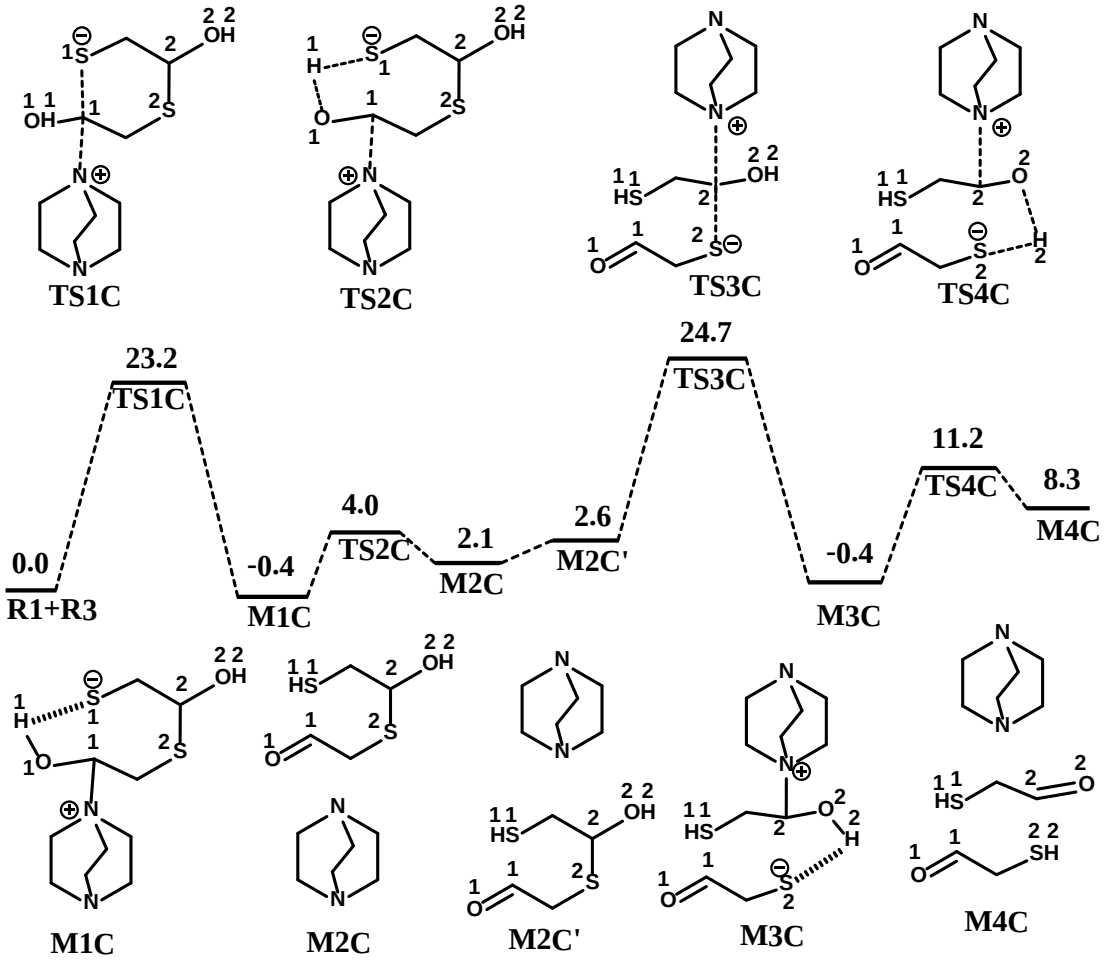

Scheme 3. The energy profile for DABCO-catalyzed cleavage of 1,4-dithiane-2,5-diol (pathway 1C), R3 represents DABCO.

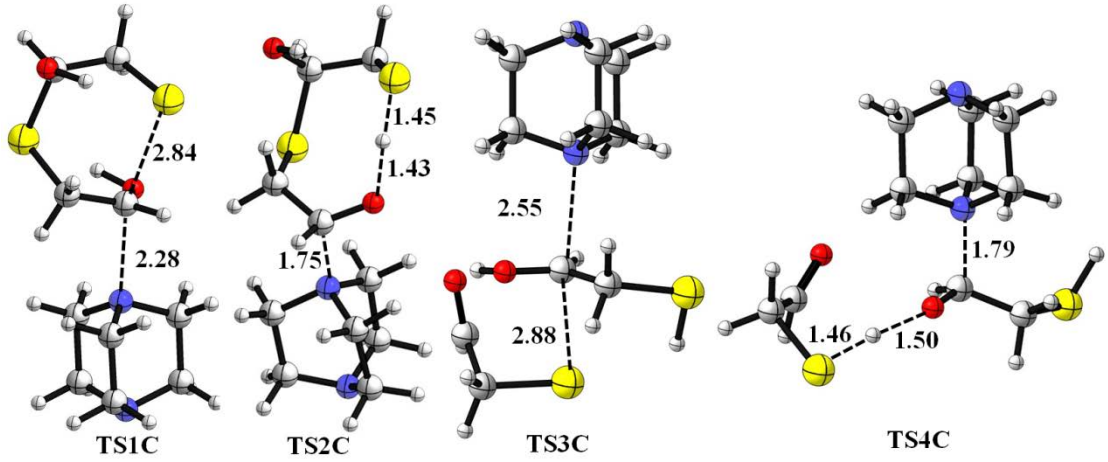

Figure 2. The optimized transition state structures for pathway 1C, selected distances are shown in Å.

1.3. **Methanol-catalyzed cleavage of 1,4-dithiane-2,5-diol**. As mentioned earlier, the title reaction is highly dependent on the solvent used, and protic solvent methanol was the best choice for this transformation in terms of both the reaction rate and yield. Furthermore, protic solvent has been demonstrated to be able to assist the proton transfer in many reactions.[65-68] In terms of these reasons, we suspect that methanol can also catalyze the cleavage of 1,4-dithiane-2,5-diol. Shown in Scheme 4 is the proposed unimolecule methanol mediated cleavage of 1,4-dithiane-2,5-diol, *i.e.* pathway 1D. As can be seen, pathway 1D consists of two reaction steps. The first step go through transition state **TS1D**, which involves C1–S1 bond breaking and two proton transfer events, i.e., proton H1 transferring from oxygen O1 to O3 atom on the hydroxyl group of methanol coupled with H3 on the hydroxyl group of methanol transferring to sulfur S1 atom. **TS1D** (shown in Figure 3) is a six-membered transition state, in which a hydrogen bond network is formed. As demonstrated in Scheme 4, the activation energy for this step amounts to 21.3 kcal/mol, which is not a high barrier at room temperature. In the generated intermediate **M1D**, O3 is hydrogen bonded with H3 and O1 is hydrogen bonded with H1. Subsequently, in order to assist the proton transfer process in the following step, the methanol molecule should be set at an appropriate position to fit the new reaction coordinate. In the present study, intermediate **M1D′** was located, in which the hydroxyl group of methanol is hydrogen bonded with H2 and S2. Then, the second reaction step takes place via transition state **TS2D**, which involves the second C–S bond breaking coupled with two proton transfer events. **TS2D** is also a six-membered transition state with an activation

energy of 26.7 kcal/mol. The optimized transition state structures for **TS1D** and **TS2D** are shown in Figure 3, in which selected key distances between pairs of atoms for **TS1D** and **TS2D** are depicted. As can be seen, each reaction step involves two proton transfer events occurring not synchronously, but rather asynchronously. The highest energy barrier in pathway 1D is 26.7 kcal/mol involving transition state **TS2D**, demonstrating that the methanol-mediated cleavage of 1,4-dithiane-2,5-diol is more energetically favorable than the direct cleavage pathways 1A and 1B.

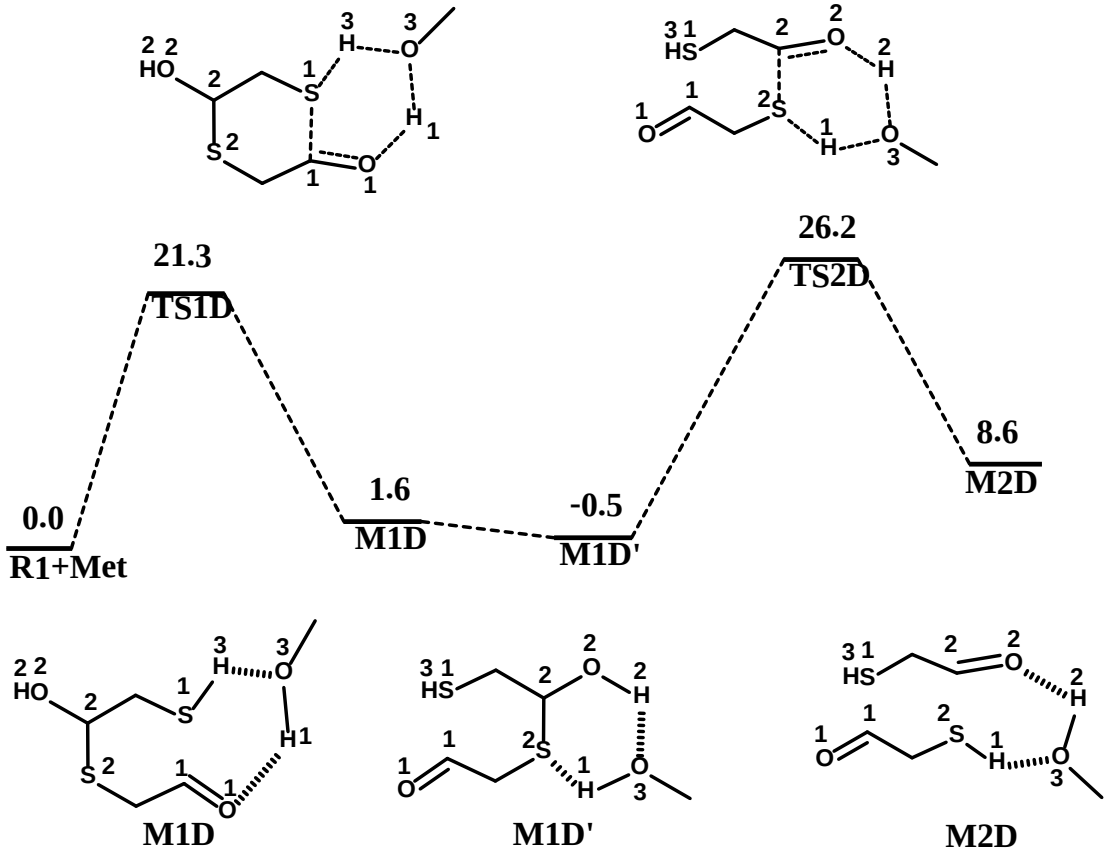

Scheme 4. The energy profile for methanol-mediated cleavage of 1,4-dithiane-2,5-diol (pathway 1D).

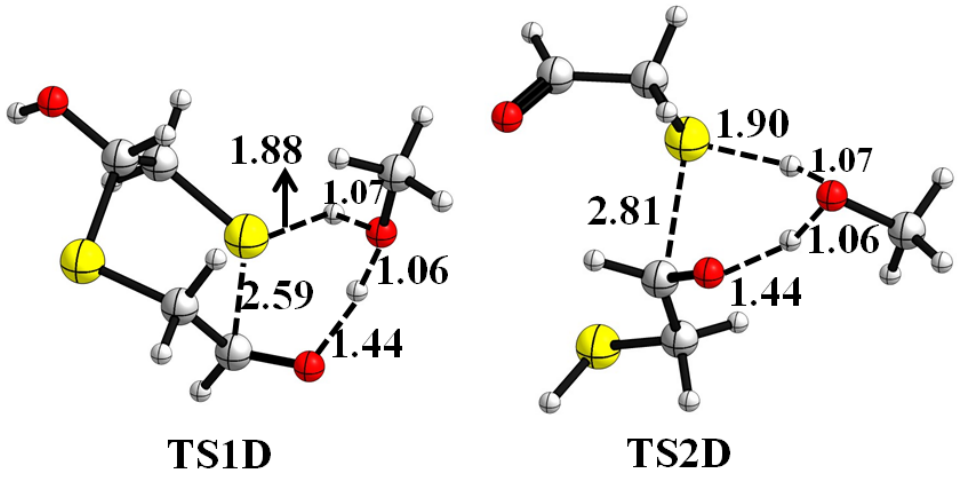

Figure 3. The optimized transition state structures for pathway D, selected distances are shown in Å.

1.4. **Double methanol-catalyzed cleavage of 1,4-dithiane-2,5-diol**. On account of methanol as the reaction solvent, two methanol molecules participating in the process for cleavage of 1,4-dithiane-2,5-diol was also taken into consideration, *i.e.* pathway 1E. In the case of two participating methanol molecules, the reaction also consists of two steps. The first step takes place via an eight-membered transition state **TS1E** with an activation energy of 8.7 kcal/mol. As can be seen from Scheme 5, **TS1E** involves one C–S bond breaking and three proton transfer events. During this reaction process, accompanied by the C1–S1 bond breaking, proton H1 of **R1** transfers to oxygen O3 atom of the first methanol molecule. Simultaneously, H3 attached with O3 transfers to O4 of the second methanol molecule, coupled with H4 attached with O4 transferring to sulfur S1 atom. **TS1E** has a big hydrogen bond network in which the distances of C1–S1, O1–H1, H1–O3, O3–H3, H3–O4, O4–H4, and H4–S1 are 2.62, 1.51, 1.03, 1.21, 1.20, 1.03 and 2.00 Å, respectively. The first step give rise to intermediate **M1E**,

in which O1 is hydrogen bonded with H1 and O4 is hydrogen bonded with H4. Similar with pathway 1D, in order to assist the proton transfer process in the following step, the two methanol molecules should also be repositioned. Correspondingly, intermediate **M1E′** was identified, in which sulfur S2 is hydrogen bonded with H1 and oxygen O4 is hydrogen bonded with H2. Next, the breaking of the second C–S bond via transition state **TS2E** gives rise to mercaptoacetaldehyde. During this reaction process, C2–S2 bond is breaking, proton H2 transfers to O4 atom, H3 returns to O3, and H1 transfers to S2 atom. In **TS2E**, the distances of C2–S2, S2–H1, H1–O3, O3–H3, H3–O4, O4–H2, and H2–O2 are 2.72, 2.02, 1.03, 1.21, 1.19, 1.03 and 1.53 Å, respectively. According to the calculated results shown in Scheme 5, this reaction step needs an activation energy of 19.9 kcal/mol, which is also the highest energy barrier in pathway 1E.

In summary, the reaction barrier for cleavage of 1,4-dithiane-2,5-diol (as summarized in Scheme 2–5) clearly decreases from 52.3 kcal/mol in single proton transfer pathway 1A to 38.6 kcal/mol in one-step cleavage pathway 1B, to 26.7 kcal/mol in methanol-mediated double proton transfer pathway 1D, and to 19.9 kcal/mol in two methanol molecules mediated triple proton transfer pathway 1E. The gradual decreasing reaction energy barriers are attributed to the reduced ring strain in the associated transition states. In the case of pathway 1A, an unfavorable four-membered transition state is encountered, while in pathway 1B, transition state **TS1B** contains two five-membered rings, in which the ring strain is reduced to some extent in comparison to the four-membered ring. Likewise, it is not surprising as one

can suspect the double proton transfer reaction pathway 1D as well as the triple proton transfer reaction pathway 1E mediated by methanol molecules to be favored most attributed also from ring strain considerations.

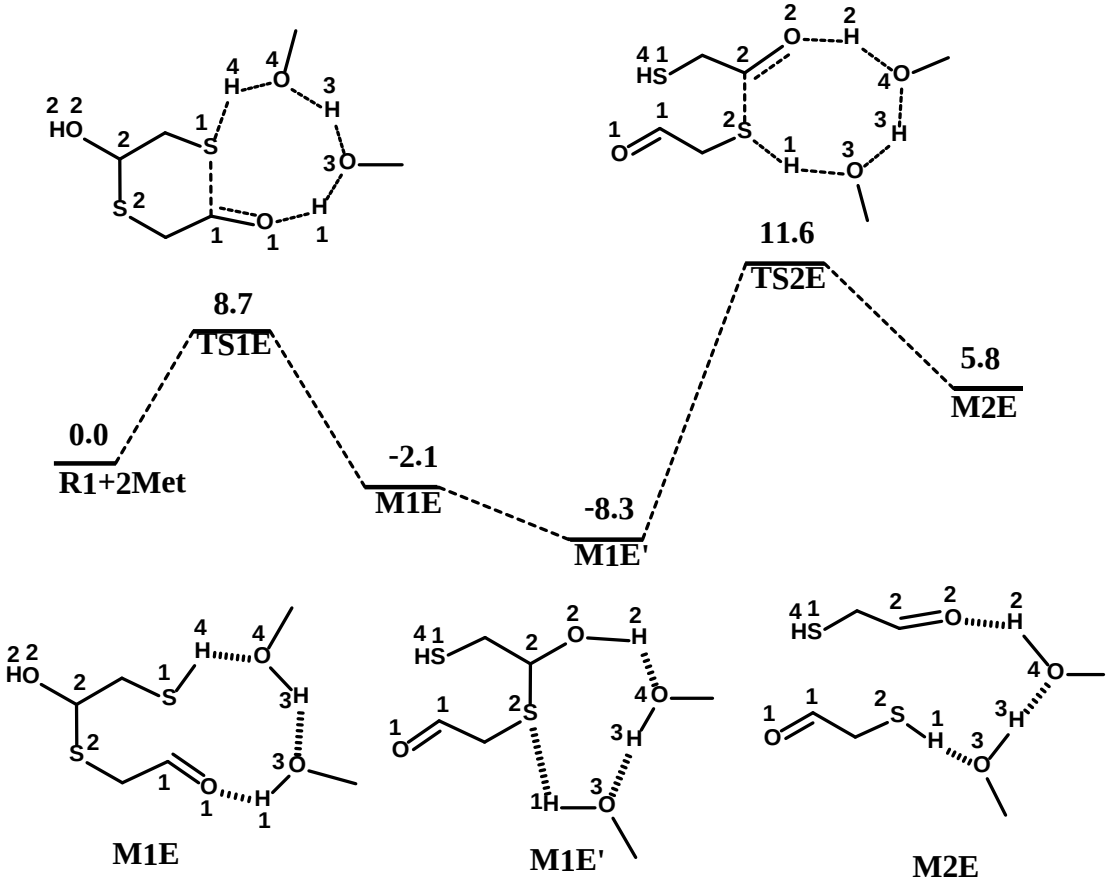

Scheme 5. The energy profile for double methanol-mediated cleavage of 1,4-dithiane-2,5-diol (pathway 1E).

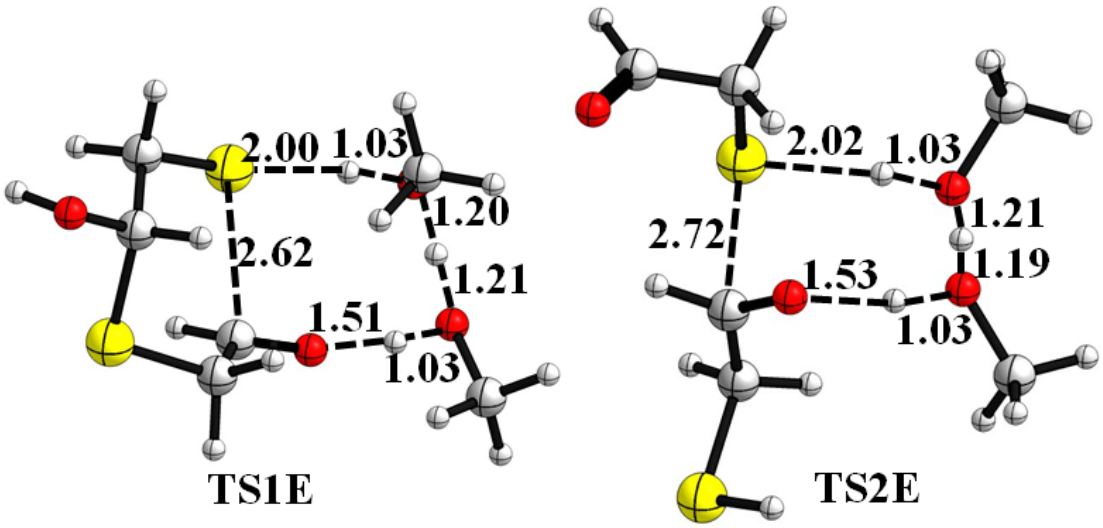

Figure 4. The optimized transition state structures for pathway 1E, selected distances are shown in Å.

2. **The [3 + 3] cycloaddition between mercaptoacetaldehyde and azomethine imines.**

For the [3 + 3] cycloaddition between mercaptoacetaldehyde and azomethine imines, three reaction pathways (pathway 2F and 2G in the absence of catalyst DABCO and pathway 2H in the presence of catalyst DABCO) were identified. In the following, all the three possible reaction pathways were discussed in detail.

2.1. The [3 + 3] cycloaddition without catalyst DABCO. In pathway 2F, the reaction is initiated with the nucleophilic attack of the negative nitrogen atom N2 of **R2** to the carbonyl carbon atom C1 of **M2**. As shown in Scheme 6, attack from the *Re* or *Si* face of **M2** can lead to the formation of intermediate **M3F1** or **M3F2**, in which the chirality of C1 is represented as *S* or *R*, respectively. Noteworthy, the nucleophilic attack in this step is accompanied by the hydrogen shift from S1 to O1. The distances of N2–C1, O1–H1, and S1–H1 in **TS3F1** and **TS3F2** (depicted in Figure 5) indicate

that O1–H1 bond formation is much more advanced than the N2–C1 bond formation. The activation energies for **TS3F1** and **TS3F2** amount to 12.5 and 15.0 kcal/mol, which are not high barriers at room temperature. Followed by the generation of **M3F1** and **M3F2** is the intramolecular cyclization via S1–C2 bond formation, resulting into the final products **P1** and **P2**. In the corresponding transition state **TS4F1** and **TS4F2**, the S1–C2 bond distance is 3.12 and 3.40 Å, respectively. This step requires an activation energy of 5.6 and 2.9 kcal/mol, indicating that it is easily to occur. On the whole, the rate-determining step in pathway F is the first step with energy barrier of 12.5 and 15.0 kcal/mol, respectively, indicating that pathway F is very competitive at room temperature.

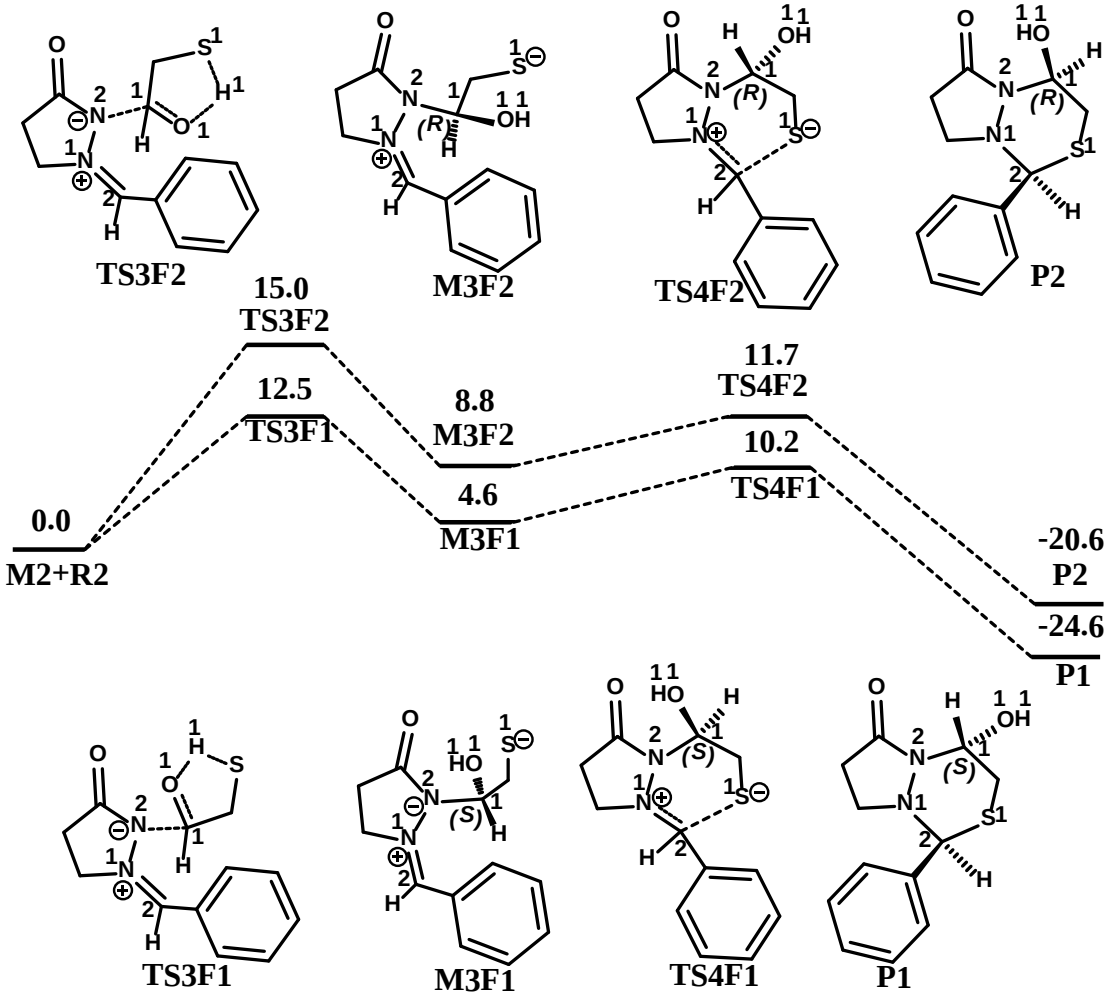

Scheme 6. The energy profile for pathway 2F.

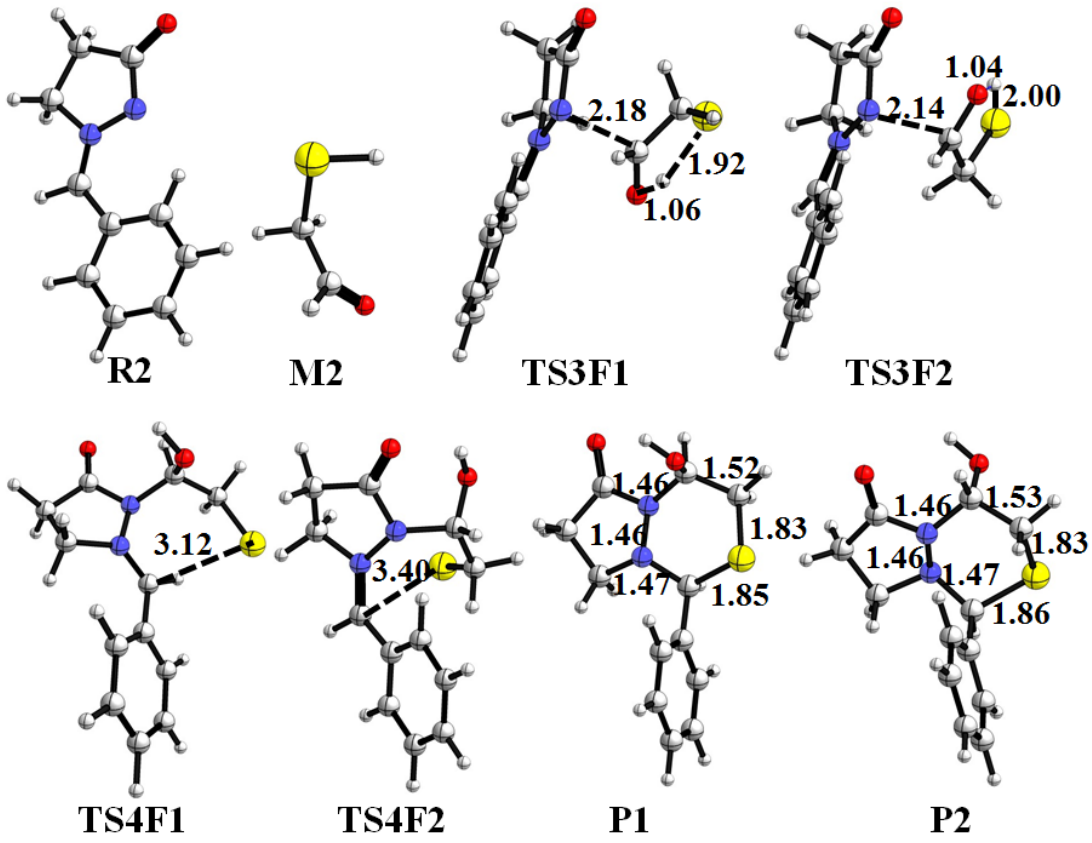

Figure 5. The optimized stationary points in pathway 2F, selected distances are shown in Å.

Different from pathway 2F, pathway 2G is initiated with the nucleophilic attack of S1 atom of **M2** to C2 atom of **R2** via transition state **TS3G**. As can be seen from Scheme 7, this reaction process involves two elementary steps, *i.e.*, nucleophilic addition and hydrogen shift. In **TS3G**, the distances of C2–S1, N2–H1, and S1–H1 are 2.77, 1.04, and 2.55 Å, respectively, indicating that N2–H1 bond formation is much more advanced than the C2–S1 bond formation. The first reaction step requires

an activation energy of 10.3 kcal/mol with respect to **M2+R2** and produces a stable intermediate **M3G**. Next, the six-membered ring cyclizatioin via N2–C1 bond formation and proton H1 transfer from N2 to O1 can give rise to the final product. Noteworthy, there are two cyclization modes via two competitive stereoisomeric transition states **TS4G1** and **TS4G2** leading to two diastereoisomeric products **P1** and **P2**. As shown in Scheme 7 and Figure 6, both the two transition states involve four-membered rings and their energy barriers are as high as 38.0 and 44.5 kcal/mol, respectively. The high energy barriers demonstrate that pathway 2G is not energy-favored.

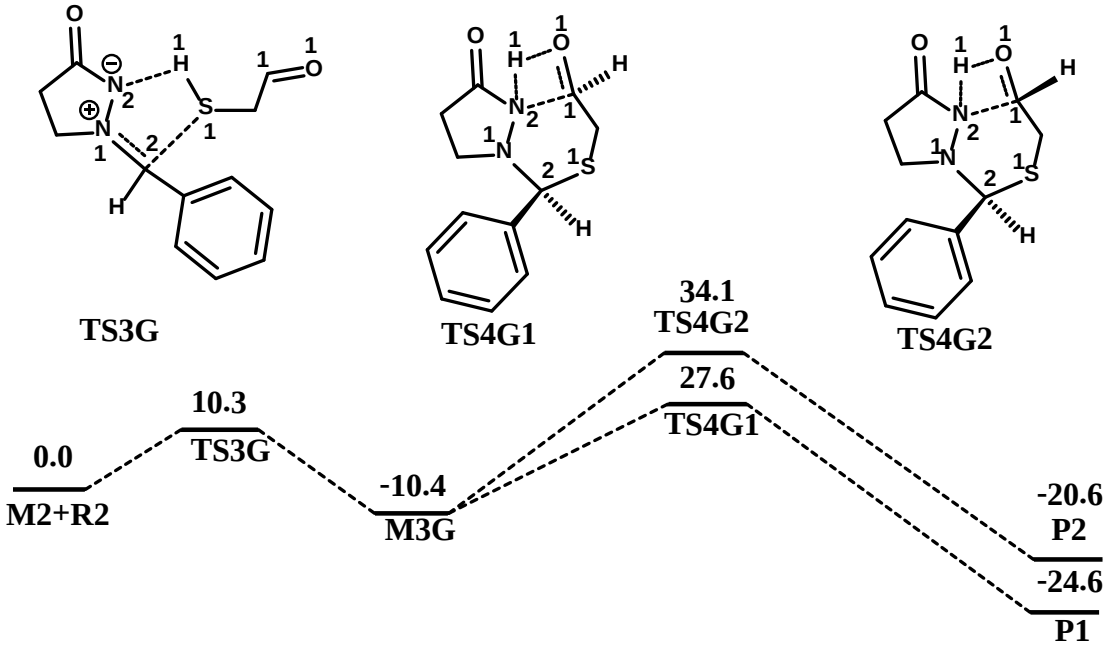

Scheme 7. The energy profile for pathway 2G.

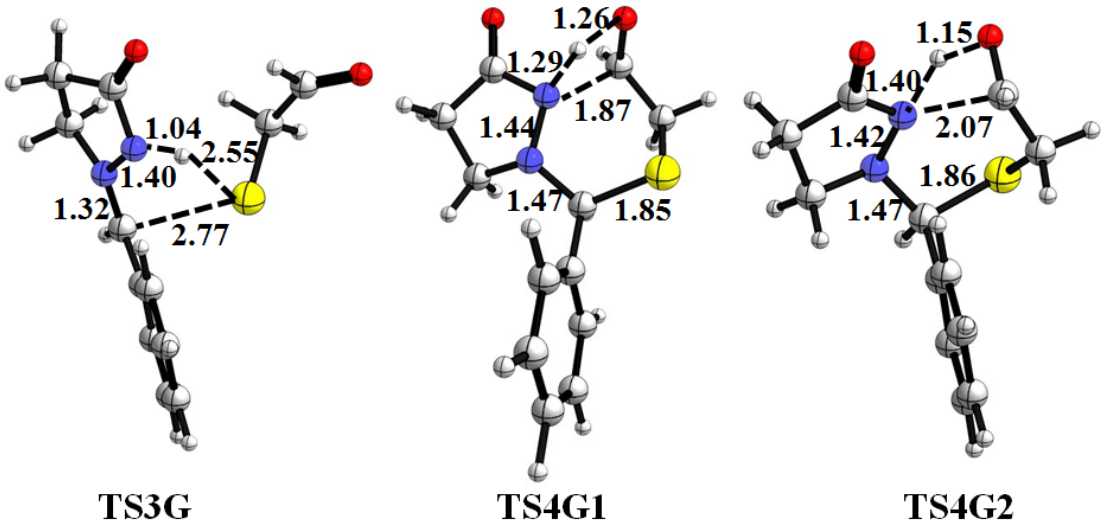

Figure 6. The optimized transition state structures in pathway 2G, selected distances are shown in Å.

2.2. DABCO-catalyzed [3 + 3] cycloaddition. As described above, DABCO may function as a general base to abstract the hydrogen H1 from sulfur S1 atom in **M2** to enhance its nucleophilicity. Herein, this proposal is also taken into consideration in the mechanistic study, and all the associated stationary points were optimized. In all, the DABCO-catalyzed [3 + 3] cycloaddition between mercaptoacetaldehyde and azomethine imines includes three reaction steps (shown in Scheme 8). At first, DABCO abstract the hydrogen H1 from sulfur S1 of **M2** and leads to intermediate **M3H**. According to our calculated results, this reaction process is barrierless and the generated intermediate **M3H** is 9.3 kcal/mol lower than **R2+M2**. **M3H** is a zwitterionic intermediate, in which nitrogen N3 atom is positive while sulfur S1 is negative and hydrogen bonded with hydrogen H1. In the following, the negative S1 atom is able to nucleophilic attack on the C2 atom of **R2** via transition state **TS4H**. The energy barrier for this step is only 2.0 kcal/mol, indicating that it is very easy to

occur. The calculated results also demonstrate that along with the nucleophilic attack of S1 on C2, H1 is gradually approaching the negative N2 atom. Therefore, in the generated intermediate **M4H**, the protonated DABCO is no longer hydrogen bonded with sulfur S1 but instead it forms a hydrogen bond with nitrogen N2. This phenomenon is a litter different from Wang's proposal, for which the protonated DABCO is hydrogen bonded with O1 of the carbonyl group in **M4H**. However, we think this hydrogen bonding mode is reasonable since it is advantageous for stabilization of the developed negative charge on N2 of **M4H**. Then, the negative nitrogen N2 would nucleophilic attack on C1 and oxygen O1 would abstract proton H1 from N3. The computational results indicate that the C1–N2 bond formation is coincident with the proton transfer from N3 to O1. Notably, there are also two competitive stereoisomeric cyclization modes via transition states **TS5H1** and **TS5H2**, in which the protonated DABCO become hydrogen bonded with O1 although at different orientations (as shown in Figure 7). The energy barrier for **TS5H1** (6.9 kcal/mol) is 3.3 kcal/mol lower than that of **TS5H2** (10.2 kcal/mol), indicating that the cyclization mode via **TS5H1** is more energetically favorable than that via **TS5H2**.

In comparison, although pathway 2F is very competitive, pathway 2H should be most energetically favorable in all the three possible reaction pathways. Apparently, **P1** derived from **TS5H1** should be the major product and **P2** derived from **TS5H2** is the minor product, which is in agreement with the experimental observation.

In summary, the first reaction of this titled domino process, i.e., the generation of mercaptoacetaldehyde, should be rate-determining. According to our calculated results, in the absence of DABCO and protic solvent, the reaction energy barrier for the title reaction amounts to 38.6 kcal/mol (associated with **TS1B**), in agreement with the experimental observation that the reaction can proceed very slowly (two days) with low yields. In the presence of DABCO and absence of protic solvent, the highest activation energy for the title reaction is calculated to be 25.1 kcal/mol (associated with **TS3C**), which is also consistent with the fact that the reaction can proceed smoothly under this condition at room temperature. Finally, with methanol as solvent and DABCO as base catalyst, the highest energy barrier for the title reaction can be further reduced to 19.9 kcal/mol (associated with **TS2E**), which is in excellent accordance with the experimental observation that the reaction can proceed efficiently under this condition. In total, our calculated results can explain all the experimental observations, indicating that the calculated results should be reasonable. Moreover, the 3.3 kcal/mol energy difference between **TS5H1** and **TS5H2** can explain the 20/1 diastereoselectivity of **P1/P2**. Structural analysis of **TS5H1** and **TS5H2** reveals that it is the larger hydrogen bonding interactions of N3–H1⋯N2 and N3–H1⋯O1 in the former case (shown in Figure 7) that determines the diastereoselectivity.

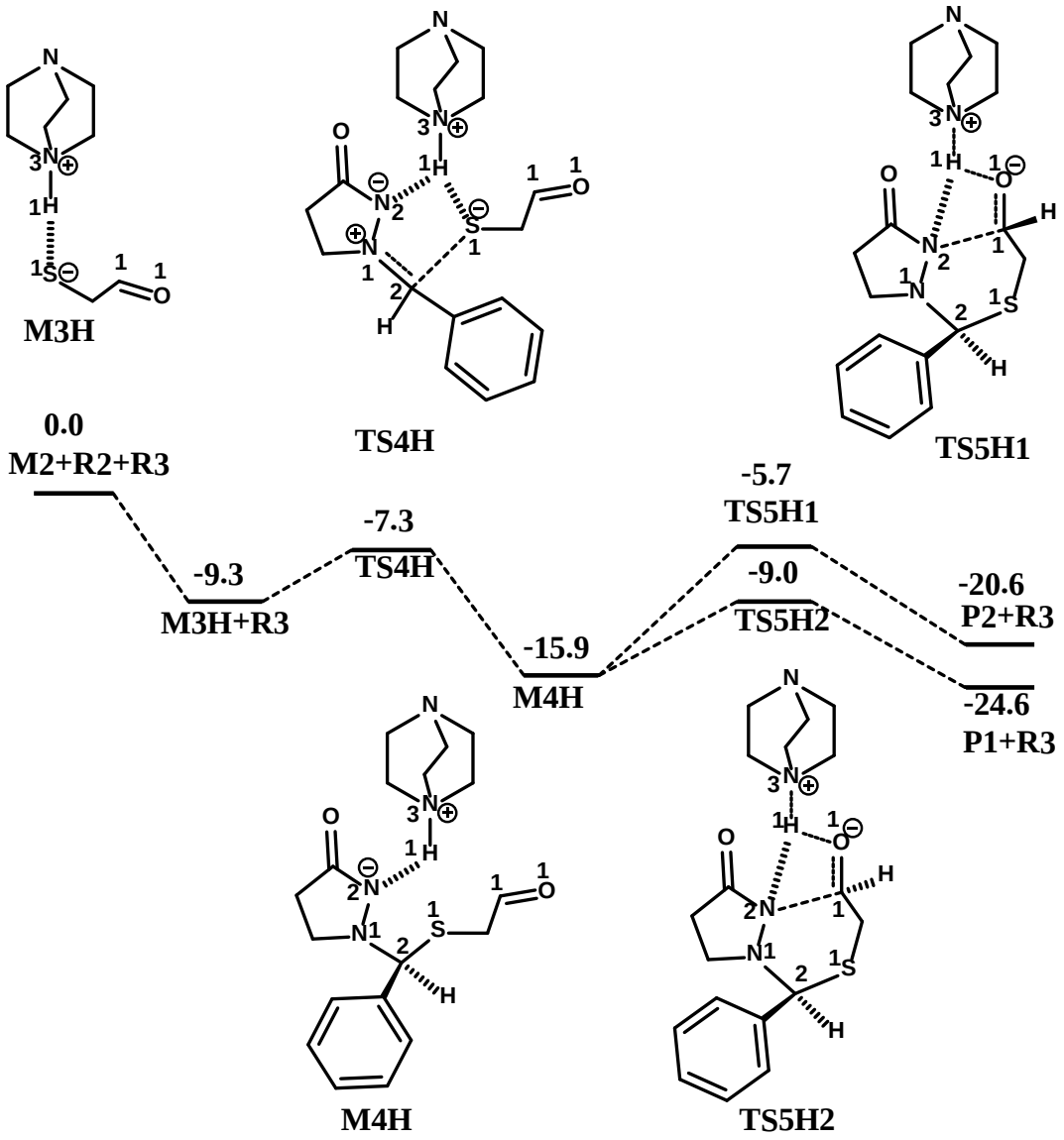

Scheme 8. The energy profile for DABCO-catalyzed [3+3] cycloaddition between mercaptoacetaldehyde and azomethine imines, R3 represents DABCO.

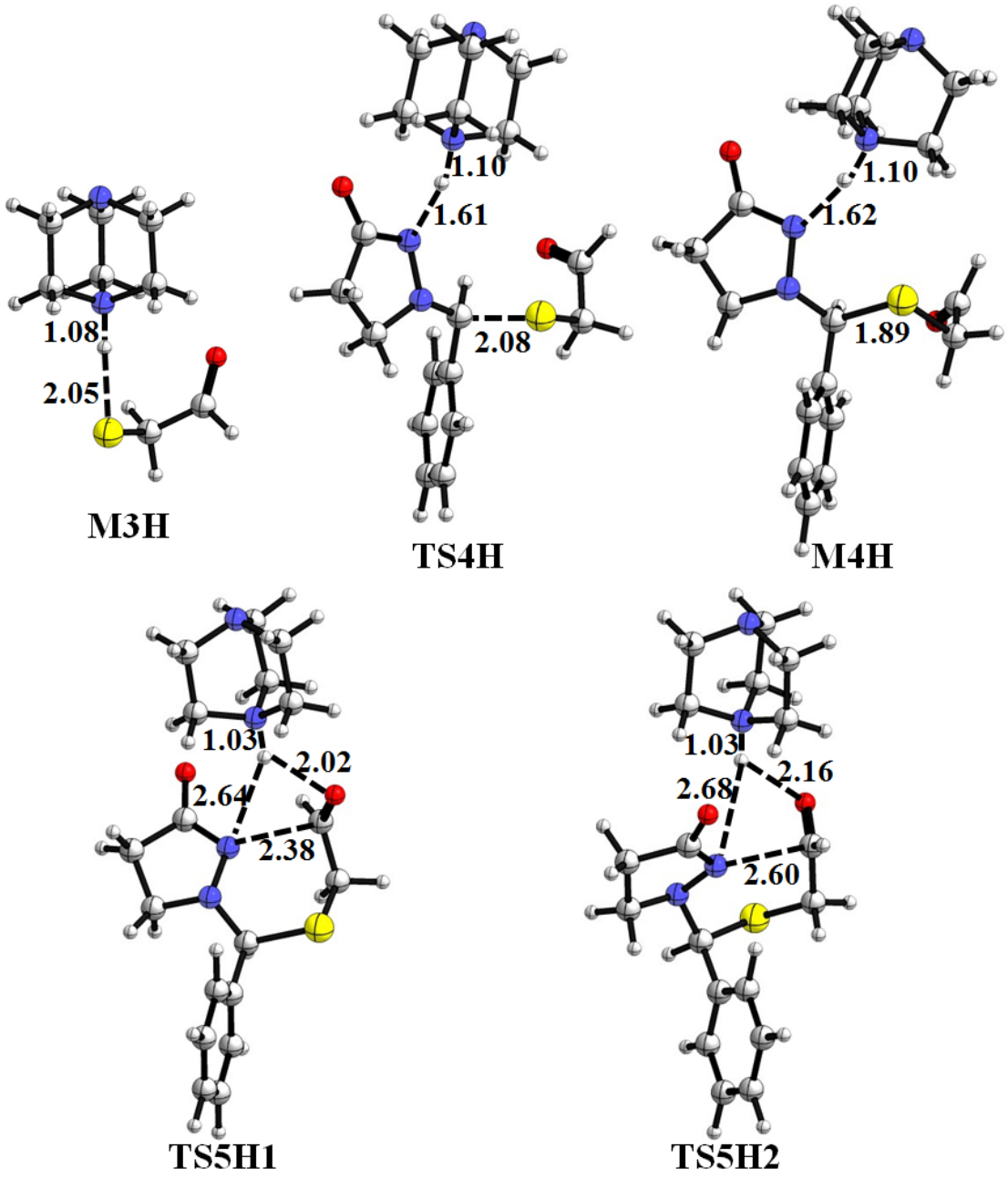

Figure 7. The optimized transition state and intermediate structures in DABCO-catalyzed [3+3] cycloaddition pathway 2H, selected distances are shown in Å.

Conclusion

In the present study, a full scenario of the reaction between

1,4-dithiane-2,5-diol and azomethine imines in methanol catalyzed by DABCO was depicted using density functional theory (DFT). The detailed reaction mechanisms as well as the diastereoselectivity of the products are analyzed. Generally speaking, the domino process consists of two consecutive reactions, generation of mercaptoacetaldehyde and [3+3] cycloaddition of mercaptoacetaldehyde with azomethine imines.

For the first reaction of this domino process, several competitive reaction pathways (1A–1E) were taken into consideration. Our calculated results reveal that both DABCO and methanol can catalyze the cleavage of 1,4-dithiane-2,5-diol and lower the energy barrier efficiently. However, DABCO and methanol catalyze the reaction in different ways. DABCO acts as a nucleophile to attack the carbon atom and enforce the C–S bond breaking, while methanol's function is to mediate the proton transfer process. The calculated potential energy profiles indicate that the double methanol molecule mediated cleavage of 1,4-dithiane-2,5-diol is most energy favorable with an activation energy of 19.9 kcal/mol. For the second reaction of this domino process, *i.e.*, [3+3] cycloaddition of mercaptoacetaldehyde with azomethine imines, three reaction pathways (with and without DABCO) were identified and DABCO-catalyzed pathway was found to be more energetically favorable than the other two. In the DABCO-catalyzed reaction pathway, DABCO acts as a general base to abstract the hydrogen from mercaptoacetaldehyde to enhance its nucleophilicity. This reaction pathway comprise three elementary steps including deprotonation of mercaptoacetaldehyde, nucleophilic attack of sulfur

anion on azomethine imines followed by intramolecular cyclization coupled with proton transfer giving rise to the final products. Moreover, there are two cyclization modes with activation energies of 6.9 and 10.2 kcal/mol. Consistent with the experimental results, the cyclization mode with lower activation energy leads to the experimentally observed major product **P1**, in which the hydroxyl group is preferentially arranged at the axial orientation. While the cyclization mode with higher activation energy leads to the experimentally observed minor product **P2**, in which the hydroxyl group is positioned not at the axial orientation but at the less hindered equatorial orientation. Furthermore, the 3.3 kcal/mol energy barrier difference can explain the product ratio of 20/1. Based on the structural analysis on the key transition states **TS5H1** and **TS5H2**, we propose that the stronger hydrogen bonding interactions in **TS5H1** results in the observed diastereoselectivity.

Acknowledgements

This work was supported financially by the National Natural Science Foundation of China (no. 21403199) and China Postdoctoral Science Foundation (no. 2014M552010)

Reference

(1) A. Nudelman, *The chemistry of optically active sulfur compounds*; Gordon and Breach: New York, 1984.

(2) *Sulphur-containing drugs and related organic compounds*. L. A. Damani, Ed.; Wiley: New York, 1989.

(3) J. Clayden, P. B. MacLellan, *J. Org. Chem.* 2011, *7*, 582-595.

(4) P. Chauhan, S. Mahajan, D. Enders, *Chem. Rev.* 2014, *114*, 8807-8864.

(5) L. Yao, K. Liu, H. Y. Tao, G. F. Qiu, X. Zhou, C. J. Wang, *Chem. Commun.* 2013, *49*, 6078-6080.

(6) R. Helder, R. Arends, W. Bolt, H. Hiemstra, H. Wynberg, *Tetrahedron Lett.* 1977, *18*, 2181-2182.

(7) X. Q. Dong, X. Fang, C. J. Wang, *Org. Lett.* 2011, *13*, 4426-4429.

(8) X. Fang, J. Li, C. J. Wang, *Org. Lett.* 2013, *15*, 3448-3451.

(9) X. Fang, X. Q. Dong, Y. Y. Liu, C. J. Wang, *Tetrahedron Lett.* 2013, *54*, 4509-4511.

(10) X. Q. Dong, X. Fang, H. Y. Tao, X. Zhou, C. J. Wang, *Chem. Commun.* 2012, *48*, 7238-7240.

(11) P. McDaid, Y. Chen, L. Deng, *Angew. Chem. Int. Ed.* 2002, *41*, 338-340.

(12) M. Moccia, F. Fini, M. Scagnetti, M. F. Adamo, *Angew. Chem. Int. Ed.* 2011, *50*, 6893-6895.

(13) G. K. Ingle, M. G. Mormino, L. Wojtas, J. C. Antilla, *Org. Lett.* 2011, *13*, 4822-4825.

(14) X. Fang, Q. H. Li, H. Y. Tao, C. J. Wang, *Adv. Synth. Catal.* 2013, *355*, 327-331.

(15) X. Tian, Y. Liu, P. Melchiorre, *Angew. Chem. Int. Ed.* 2012, *51*, 6439-6442.

(16) Q.-L. Pei, H.-W. Sun, Z.-J. Wu, X.-L. Du, X.-M. Zhang, W.-C. Yuan, *J. Org. Chem.* 2011, *76*, 7849-7859.

(17) J. Sun, G. C. Fu, *J. Am. Chem. Soc.* 2010, *132*, 4568-4569.

(18) Y. Fujiwara, J. Sun, G. C. Fu, Chem. Sci. 2011, 2, 2196-2198.

(19) T. Honjo, S. Sano, M. Shiro, Y. Nagao, *Angew. Chem. Int. Ed.* 2005, *44*, 5838-5841.

(20) A. Peschiulli, C. Quigley, S. Tallon, Y. K. Gun'ko, S. J. Connon, *J. Org. Chem.* 2008, *73*, 6409-6412.

(21) A. Peschiulli, B. Procuranti, O. C. CJ, S. J. Connon, *Nat. Chem.* 2010, *2*, 380-384.

(22) Z. B. Luo, X. L. Hou, L. X. Dai, *Tetrahedron: Asymmetry* 2007, *18*, 443-446.

(23) G. Della Sala, A. Lattanzi, *Org. Lett.* 2009, *11*, 3330-3333.

(24) G. Della Sala, *Tetrahedron* 2013, *69*, 50-56.

(25) Z. Wang, Z. Chen, J. Sun, *Angew. Chem. Int. Ed.* 2013, *52*, 6685-6688.

(26) Z. Rodriguez-Docampo, C. Quigley, S. Tallon, S. J. Connon, *J. Org. Chem.* 2012, *77*, 2407-2414.

(27) Z. C. Geng, N. Li, J. Chen, X. F. Huang, B. Wu, G. G. Liu, X. W. Wang, *Chem. Commun.* 2012, *48*, 4713-4715.

(28) S. Sobhani, D. Fielenbach, M. Marigo, T. C. Wabnitz, K. A. Jorgensen, *Chemistry* 2005, *11*, 5689-5694.

(29) L. Fang, A. Lin, H. Hu, C. Zhu, *Chemistry* 2009, *15*, 7039-7043.

(30) Wang, C.; Yang, X.; Loh, C. C.; Raabe, G.; Enders, D. *Chemistry* 2012, *18*, 11531-11535.

(31) Y. Kageyama, S. Murata, *J. Org. Chem.* 2005, *70*, 3140-3147.

(32) S. S. Sohn, J. W. Bode, *Angew. Chem. Int. Ed.*2006, *45*, 6021-6024.

(33) T. Uno, T. Inokuma, Y. Takemoto, *Chem. Commun.* 2012, *48*, 1901-1903.

(34) X. Fang, J. Li, H. Y. Tao, C. J. Wang, *Org. Lett.* 2013, *15*, 5554-5557.

(35) X. Xu, M. P. Doyle, *Acc. Chem. Res.* 2014, *47*, 1396-1405.

(36) E. M. Kosower, A. E. Radkowsky, A. H. Fairlamb, S. L. Croft, R. A. Nea, *Eur. J. Med. Chem.* 1995, *30*, 659-671.

(37) S. Hanessian, G. McNaughton-Smith, H.-G. Lombart, W. D. Lubell, *Tetrahedron* 1997, *53*, 12789-12854.

(38) G. Sathishkannan, K. Srinivasan, *Chem. Commun.* 2014, *50*, 4062-4064.

(39) J. B. Ling, Y. Su, H. L. Zhu, G. Y. Wang, P. F. Xu, *Org. Lett.* 2012, *14*, 1090-1093.

(40) S. W. Duan, Y. Li, Y. Y. Liu, Y. Q. Zou, D. Q. Shi, W. J. Xiao, *Chem. Commun.* 2012, *48*, 5160-5162.

(41) D. C. Fang, Y. M. Chen, *Acta Chim. Sinica* 2014, *72*, 253-256.

(42) D. C. Fang, *Prog. Chem.* 2012, *24*, 879-885.

(43) Y. M. Xing, L. Zhang, D. C. Fang, *Organometallics* 2015, *34*, 770-777.

(44) Q. Zhang, H.-Z. Yu, Y. Fu, *Org. Chem. Front.* 2014, *1*, 614-620.

(45) L. R. Domingo, R. J. Zaragoza, M. Arno, *Org. Biomol. Chem.* 2010, *8*, 4884-4891.

(46) L. R. Domingo, R. J. Zaragoza, J. A. Saez, M. Arno, *Molecules* 2012, *17*, 1335-1353.

(47) L. R. Domingo, M. J. Aurell, P. Perez, J. A. Saez, *Rsc Adv.* 2012, *2*, 1334-1342.

(48) M. Esseffar, R. Jalal, M. J. Aurell, L. R. Domingo, *Comput. Theor. Chem.* 2014, *1030*, 25-32.

(49) L. H. Yang, Y. L. Yuan, H. M. Wang, N. Zhang, S. G. Hong, *Rsc Adv.* 2014, *4*, 32457-32466.

(50) L. H. Yang, H. M. Wang, N. Zhang, S. G. Hong, *Dalton Trans.* 2013, *42*, 11186-11193.

(51) Y. Qiao, K. L. Han, *Org. Biomol. Chem.* 2012, *10*, 7689-7706.

(52) Y. Qiao, K. L. Han, *Org. Biomol. Chem.* 2014, *12*, 1220-1231.

(53) Y. Qiao, T. S. Chu, *J. Org. Chem.* 2011, *76*, 3086-3095.

(54) M. J. Frisch, G. W. Trucks, H. B. Schlegel, G. E. Scuseria, M. A. Robb, J. R. Cheeseman, J. A. Montgomery Jr, T. Vreven, K. N. Udin, J. C. Burant, J. M. Millam, S. S. Yengar, J. Tomasi, V. Barone, B. Mennucci, M. Cossi, G. Scalmani, N. Rega, G. A. Petersson, H. Nakatsuji, M. Hada, M. Ehara, K. Toyota, R. Fukuda, J. Hasegawa, M. Shida, T. Nakajima, Y. Honda, O. Kitao, H. Nakai, M. Klene, X. Li, J. E. Knox, H. P. Hratchian, J. B. Cross, V. Bakken, C. Adamo, J. Jaramillo, R. Gomperts, R. E. Stratmann, O. Yazyev, A. J. Austin, R. Cammi, C. Pomelli, J. W. Ochterski, P. Y. Ayala, K. Morokuma, G. A. Voth, P. Salvador, J. J. Dannenberg, V. G. Zakrzewski, S. Dapprich, A. D. Daniels, M. C. Strain, O. Farkas, D. K. Malick, A. D. Rabuck, K. Raghavachari, J. B. Foresman, J. V. Ortiz, Q. Cui, A. G. Baboul, S. Clifford, J. Cioslowski, B. B. Stefanov, G. Liu, A. Liashenko, P. Piskorz, I. Komaromi, R. L. Martin, D. J. Fox, T. Keith, M. A. Al-Laham, C. Y. Peng, A. Nanayakkara, M. Challacombe, P. M. W. Gill, B.nJohnson, W. Chen, M. W. Wong, C. Gonzalez, J. A. Pople, Revision A.02 ed.; Gaussian, Inc.: Wallingford CT, 2009.

(55) A. D. Becke, J. Chem. Phys. 1993, 98, 5648-5652.

(56) C. T. Lee, W. T. Yang, R. G. Parr, Phys. Rev. B 1988, 37, 785-789.

(57)W. Sang-Aroon, V. Ruangpornvisuti, *Int. J. Quantum. Chem.* 2008, *108*, 1181-1188.

(58)J. Tomasi, B. Mennucci, Cancès, E. *J. Mol. Struct-Theochem* 1999, *464*, 211-226.

(59) X. S. Li, M. J. Frisch, *J. Chem. Theory. Comput.* 2006, *2*, 835-839.

(60)C. Gonzalez, H. B. *J.* Schlegel, *Chem. Phys.* 1989, *90*, 2154-2161.

(61)C. Gonzalez, H. B. *J.* Schlegel, *Phys. Chem.* 1990, *94*, 5523-5527.

(62)Y. Zhao, D. Truhlar, *Theor. Chem. Acc.* 2008, *120*, 215-241.

(63)Y. Zhao, D. G. Truhlar, *Acc. Chem. Res.* 2008, *41*, 157-167.

(64)Y. Zhao, D. G. Truhlar, *J. Chem. Theory. Comput.* 2008, *4*, 1849-1868.

(65)B. Cheng, G. Huang, L. Xu, Y. Xia, *Org. Biomol. Chem.* 2010, *10*, 4417-4423.

(66)G. Huang, B. Cheng, L. Xu, Y. Li, Y. Xia, *Chem. Eur. J.* 2012, *18*, 5401-5415.

(67)Y. Xia, G. Huang, *J. Org. Chem.* 2010, *75*, 7842-7854.

(68)W. Guo, Y. Xia, *Synthesis* 2014, 46, 2149-2154.